"Chemically Shielded" Poly(ethylene oxide) Single Crystal Growth and Construction of Channel-Wire Arrays with Chemical and Geometric Recognitions on a Submicrometer Scale

William Y. Chen,[†] Christopher Y. Li,[‡] Joseph X. Zheng,[†] Ping Huang,[†] Lei Zhu,[§] Qing Ge,[†] Roderic P. Quirk,[†] Bernard Lotz,[||] Lingfeng Deng,[⊥] Chi Wu,[⊥] Edwin L. Thomas,[#] and Stephen Z. D. Cheng*[,†]

Maurice Morton Institute and Department of Polymer Science, The University of Akron, Akron, Ohio 44325-3909; Department of Materials Science and Engineering, Drexel University, Philadelphia, Pennsylvania 19104; Polymer Program, Institute of Materials Science and Department of Chemical Engineering, The University of Connecticut, Storrs, Connecticut 06269-3136; Institut Charles Sadron, 6 Rue Boussingault, Strasbourg 67083, France; Departments of Chemistry and Physics, Hong Kong Chinese University, Sha Tin, Hong Kong; and Department of Materials Science and Engineering, Massachusetts Institute of Technology, Cambridge, Massachusetts 02139

Received April 5, 2004; Revised Manuscript Received May 5, 2004

ABSTRACT: A series of poly(ethylene oxide)-*block*-polystyrene (PEO-*b*-PS) diblock copolymers were used to generate nucleation sites for the crystal growth of a homo-PEO fraction in solution. The number-average molecular weights of the PEO blocks (M_n^{PEO}) were similar, and the number-average molecular weights of the PS blocks (M_n^{PS}) ranged from 4.6K to 17K g/mol. In PEO-*b*-PS/(chlorobenzene/octane) solutions, square-shaped single crystals bounded by four {120} planes were isothermally grown and observed with transmission electron and atomic force microscopy. A "sandwich" lamellar structure, constructed by a PEO single crystal layer covered by two tethered PS block layers on the top and bottom crystal basal surfaces, was found. These diblock copolymer single crystals were used as seeds to grow homo-PEO (M_n^{PEO} = 56K g/mol) single crystals in amyl acetate. When the M_n^{PS} in the block copolymer was 4.6K g/mol, the edges and corners of the {120} bounded PEO-*b*-PS single crystals served as nucleation sites to initiate the further growth of the homo-PEO single crystal. As the M_n^{PS} of the block copolymers increased, the homo-PEO crystal growth was increasingly hampered along the {120} edges of the PEO-*b*-PS single crystals. When the M_n^{PS} of the block copolymer was 17K g/mol, only the four corners of the PEO-*b*-PS single crystal could still act as nucleation sites. The four edges were chemically "shielded" by the tethered PS blocks. This indicates that increasing the M_n^{PS} led to a higher reduced tethering density of the PS blocks on both the basal surfaces of the PEO-*b*-PS single crystals. The repulsion generated among the tethered PS blocks caused the PS blocks located near and at the edges to advance along the [120] direction. Interestingly, this local environment only accepted the PEO-*b*-PS molecules but rejected the homo-PEO molecules from further growth. As a direct result of this study, novel channel-wire arrays on a submicrometer length scale having chemical and geometric recognitions could be fabricated via alternating crystal growth of PEO-*b*-PS and homo-PEO. This fabrication provided robustly controlled arrays with spacing down to 50 nm.

Introduction

Polymer crystallization has been a long discussed topic in the past 50 years and described as a thermodynamic first-order transition that is a nucleation-controlled process.[1−5] The nucleation barrier controls the crystallization kinetics. However, the specific trajectory of one macromolecule among many others during crystallization may encompass multiple steps. Crystallization begins with the absorption of a part of one macromolecule and ends with the incorporation of that molecule into a crystal lattice in a chain-folded fashion. Whether or not crystallization can occur and how fast it can take place rely on several sequential and cooperative selection processes on different length and time scales. The overall effect of these selection processes on the free energy in terms of both the enthalpic and entropic contributions construct the nucleation barrier.[5] One of these selection processes is the local chemical and physical environments provided for polymer crystallization. These different environments can enhance polymer crystallization, such as crystallization from a preordered state rather than in the isotropic state,[6,7] or hamper it, such as crystallization under "self-poisoning"[8−11] or in amorphous−crystalline polymer blends[12−14] or under different nanoconfinements.[15−18]

In this publication, we report our solution crystallization experiments to create a specific chemical environment using a series of poly(ethylene oxide)-*block*-polystyrene (PEO-*b*-PS) diblock copolymers as seeds to further initiate homo-PEO crystal growth. It is known that PEO-*b*-PS diblock copolymers can crystallize in dilute solutions to grow single crystals, leading to a PEO block single crystal as the middle layer with the PS block layers are at the top and bottom of the basal surfaces (of the PEO single crystal) to form a "sandwich" structure.[19,20] The single crystals exhibit a square shape bounded by four {120} planes, identical to the homo-PEO single crystals.[21−23] If we use these PEO-*b*-PS

[†] The University of Akron.
[‡] Drexel University.
[§] The University of Connecticut.
[||] Institut Charles Sadron.
[⊥] Hong Kong Chinese University.
[#] Massachusetts Institute of Technology.
* To whom the correspondence should be addressed: e-mail scheng@uakron.edu.

10.1021/ma0493325 CCC: $27.50
Published on Web 06/18/2004

Table 1. Molecular Characterizations of PEO-*b*-PS Diblock Copolymers and Homo-PEO

samples	M_n ($\times 10^3$ g/mol)	M_n^{PEO} ($\times 10^3$ g/mol)	M_n^{PS} ($\times 10^3$ g/mol)	M_w/M_n	f_{PEO}[a]
homo-PEO	56.0	56.0	0	1.03	1
PEO-*b*-PS	15.6	11.0	4.6	1.07	0.67
PEO-*b*-PS	17.9	8.7	9.2	1.06	0.45
PEO-*b*-PS	28.0	11.0	17.0	1.07	0.35

[a] Volume fraction of PEO assuming PEO has 100% crystallinity.

single crystals as seeds to further initiate the crystal growth of homo-PEO, the lateral PEO {120} planes should serve as nucleation sites to induce the homo-PEO single crystal growth. However, since the PS blocks tethered on the top and bottom of the basal surfaces of the crystals are not solidified in dilute solution, it is interesting to investigate how the overcrowding of the PS blocks affects the homo-PEO crystal growth. Furthermore, this study results in a novel method to fabricate channel-wire arrays with chemical and geometric recognitions on a submicrometer length scale via alternatively growing the PEO-*b*-PS and homo-PEO crystals.

Experimental Section

Materials. Three PS-*b*-PEO diblock copolymers were sequentially synthesized via anionic block copolymerization of styrene and ethylene oxide. Detailed synthesis procedures were described elsewhere.[24,25] The molecular characterization data such as the number-average molecular weights of PEO blocks and PS blocks (M_n^{PEO} and M_n^{PS}), polydispersities (M_w/M_n), and volume compositions of the PEO blocks (f_{PEO}) of these three diblock copolymers are listed in Table 1. The M_n^{PS} precursors were characterized by size exclusion chromatography (SEC) using the polystyrene standards, while the M_n^{PEO} of the PEO blocks were determined by proton nuclear magnetic resonance results. The polydispersities in the final diblock copolymers were determined by SEC using, again, the universal calibration. A homo-PEO fraction was also used in this study, and its molecular characterization is also listed in Table 1.

Equipment and Experiments. Solution crystallization of PEO-*b*-PS copolymers was carried out with a dilute concentration of 0.01 wt % in a mixed solvent of chlorobenzene and octane with a 1:1.1 weight ratio. The polymer samples were put into the solvent and heated to above the dissolution temperature (T_d = 42 °C in the mixed solvent) in a temperature-controlled oil bath. Self-seeding experiments were utilized.[19,20] The procedure of this self-seeding included switching to another oil bath at room temperature for a fast crystallization of the sample and then reheating it to a seeding temperature which was 0.5 °C lower than the T_d and kept there for 20 min. The sample was then quickly cooled to a preset crystallization temperature (T_c) in another isothermal oil bath to grow single crystals. On the other hand, the PEO/amyl acetate solution (0.01 wt %) was prepared by dissolving the homo-PEO fraction in amyl acetate at 65 °C for 10 min and cooled to a preset T_c = 30 °C. This T_c was chosen since it was high enough to prevent the crystallization of homo-PEO in amyl acetate without seeds for a period of hours. The homo-PEO crystallization occurred in the amyl acetate solution only after one drop of the solution containing the PEO-*b*-PS single crystal seeds were added. The homo-PEO single crystals could then grow on the {120} growth fronts of the PEO-*b*-PS single crystals.

The alternating crystallization of the PEO-*b*-PS and homo-PEO was carried out only in amyl acetate dilute solution. This was due to the fact that homo-PEO fractions cannot grow single crystals in the mixed solvent. It was necessary to know both the growth rates of the PEO-*b*-PS (with M_n^{PS} = 4.6K g/mol) and the homo-PEO (M_n^{PEO} = 56K g/mol) at the specified T_c and concentration. We also used other homo-PEO fractions with different M_n^{PEO} values ranging from 20K to 50K g/mol, and the results were identical. The detailed procedure was that, first, the homo-PEO single crystals were grown in amyl acetate at T_c = 30 °C with the self-seeding technique. A quantitative amount of the homo-PEO single crystals suspended in the amyl acetate solution was transferred to a precooled PEO-*b*-PS/amyl acetate dilute solution for PEO-*b*-PS crystal growth on the {120} growth fronts of the homo-PEO single crystals at the same T_c. After the growth of PEO-*b*-PS was finished, the crystals were then transferred to a controlled homo-PEO/amyl acetate dilute solution, and the homo-PEO further grew on the {120} growth fronts of the preexisting crystals at the same T_c. This sequence could be repeated to achieve the alternating PEO/PEO-*b*-PS crystals.

The single crystals were washed in amyl acetate several times and placed onto carbon-coated copper grids, predried in the glovebox with N_2 flow, and further dried under vacuum for 2 days at room temperature for transmission electron microscopy (TEM) experiments. For atomic force microscopy (AFM) experiments, the samples were directly deposited on silicon wafers following the same drying procedure.

TEM experiments were carried out in a JEOL (1200 EX II) TEM using an accelerating voltage of 120 kV. To determine crystal orientation, TEM was used to obtain selected area electron diffraction (SAED) patterns of the samples. Calibration of the ED spacing was done using TlCl *d* spacings and their higher order diffractions. An AFM (Digital Instrument Nanoscope IIIA) was used in tapping mode to examine the single crystal morphology and lamellar thickness. The force applied on the cantilever was adjusted to the minimum limit, but enough to keep good engagement between AFM tip and crystal surface, to limit the damage to the sample. The scanning rate was 1 Hz for the scan size of 10 μm, and the resolution was 512 × 512. The operation and resonance frequencies were ~290 kHz. The scanner was calibrated with the standard grid for both lateral size and height.

To study chain-folding direction of the lamellar crystals, a polyethylene (PE) decoration method was utilized.[23,26,27] A linear PE sample with a M_n^{PE} of 12K g/mol and polydispersity of 1.2 was used. During the decoration of PE, an optimal 10 cm distance between the sample and the basket was chosen in the vacuum evaporator. PE was degraded to ~1K g/mol, evaporated, deposited, and crystallized on the sample surfaces.

Results and Discussion

PEO-*b*-PS "Sandwiched" Single Crystals. Figure 1 shows a square-shaped single crystal of PEO-*b*-PS with M_n^{PS} = 4.6K g/mol in a bright field (BF) TEM image with an insert of a SAED pattern of this crystal in the correct orientation. It was crystallized at T_c = 30 °C in chlorobenzene/octane after following the self-seeding procedure. The two pairs of strongest diffraction spots, which are perpendicular to each other, are attributed to the {120} planes, indicating that the PEO chain direction is parallel to the electron beam (i.e., parallel to the lamellar normal). This SAED pattern is thus the [001] zone of the PEO single crystal. Identical to the previously observed morphology, the four edges of this single crystal are bounded by four {120} planes, which are crystal growth fronts with the slowest growth rate during the crystallization.[20−22] The weak diffractions of the (200), (240), and (040) planes in this SAED pattern can also be observed, confirming the monoclinic PEO crystal structure.[28]

Furthermore, Figure 1 shows a PEO-*b*-PS single crystal after the PE decoration. A number of low molecular weight PE crystal rods were observed on the top of the crystal resulting from the PE decoration. The *c*-axis of these PE crystals is perpendicular to the long axis of these rods.[23,26,27] The rods in this figure possess an isotropic (random) in-plane orientation, revealing

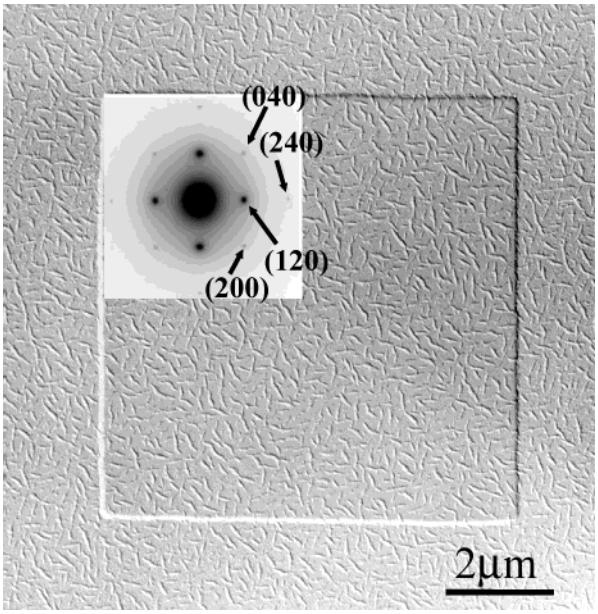

Figure 1. TEM BF image of a square-shaped "sandwiched" single crystal of a PEO-*b*-PS diblock copolymer (M_n^{PS} = 4.6K g/mol) crystallized at T_c = 30 °C in chlorobenzene/octane dilute solution after PE decoration. The inset is the [001] zone SAED of this single crystal with assignments of different crystalline planes.

that the PE was decorated on a featureless surface which is usually amorphous in nature. Note that when the "sandwiched" single crystals were precipitated onto the carbon-coated surfaces, either basal surface could face up. We have then an equal opportunity to view either side of the basal surfaces of these single crystals. Since all of our observations of these PE-decorated PEO-*b*-PS single crystals exhibit the random orientation of PE crystal rods, it can be concluded that the PS blocks cover the top and bottom of the PEO crystal basal surfaces to form the "sandwiched" structure.

Figure 2a is an AFM height image of a square-shaped PEO-*b*-PS "sandwiched" lamella with M_n^{PS} = 9.2K g/mol, which was crystallized at T_c = 30 °C after the self-seeding procedure. The overall "sandwich" thickness ($d_{overall}$) is 18.8 nm. A sample was also tilted ~30° at a temperature of 59 °C, and an AFM phase image using the tapping mode on this sample is shown in Figure 2b. The lamellar structure is observed to be constructed from three layers. Note that at 59 °C the PS layers are still below their glass transition temperature (62 °C) and the PEO crystal has melted to a liquid at 59 °C.[29] Therefore, the top and bottom PS and one sandwiched PEO layers possess different moduli and respond differently to the tapping tip of AFM.

The BF TEM experiments on the PEO-*b*-PS single crystals grown from the other two diblock copolymers in chlorobenzene/octane dilute solution also show the same square shape as is observed in Figure 1. Based on the AFM observations, the values of $d_{overall}$ of the PEO-*b*-PS single crystals with M_n^{PS} = 4.6K and 17K g/mol are 17.0 and 22.3 nm, respectively, at the same T_c. However, we observe in AFM slightly thicker edges compared with the center area thickness as shown by the height profile in Figure 3 for the M_n^{PS} = 17K g/mol PEO-*b*-PS diblock copolymer. With increasing M_n^{PS}, this phenomenon becomes more evident. The reason for the thicker edges may be that, after drying the single crystal, the PS blocks near and at the {120} edges have

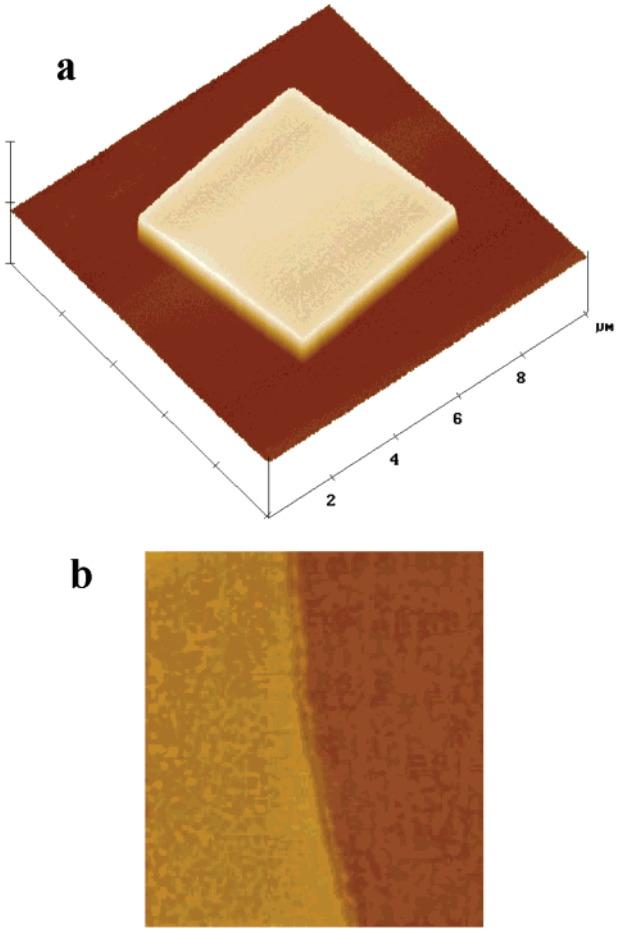

Figure 2. AFM height image of a square-shaped "sandwiched" single crystal of PEO-*b*-PS diblock copolymer under the same crystallization condition as in Figure 1a and a ~30°-tilted phase-mode AFM image of a "sandwiched" single crystal with the three-layer structure measured at 59 °C using the tapping mode (b).

smaller coverage areas per PS block on the PEO crystal basal surface compared with those in the center area (see below). The distance from the edge where the thickness starts to change is approximately 2 μm.

To calculate the thicknesses of PEO and PS layers (d_{PEO} and d_{PS}), the first assumption we made is that the density of the PS block layers is identical to that of the amorphous PS bulk (ρ_{PS} = 1.052 g/cm^{-3}).[30] The densities of the PEO crystal (ρ^c_{PEO}) and the amorphous PEO (ρ^a_{PEO}) are identical to the bulk densities of 1.239 and 1.124 g cm^{-3}, respectively, at room temperature.[30] Since the PEO crystal structure in the single crystal, as determined by the SAED experiments, is identical to that in the bulk (see the inset of Figure 1), we do not expect any deviation between the ρ^c_{PEO} values of the single crystal and the crystals in the bulk. Furthermore, the PEO blocks in this system possess a crystallinity (W^c_{PEO}, and $1 - W^c_{PEO} = W^a_{PEO}$) of 95%.[31] This minimizes deviation caused by the assumption of ρ^a_{PEO}. Since $d_{PEO} = d_{overall} V_{PEO}$ (%), and it can be expressed using the equation[32]

$$d_{PEO} = d_{overall} \frac{M_n^{PEO}/(W^c_{PEO}\rho^c_{PEO} + W^a_{PEO}\rho^a_{PEO})}{M_n^{PEO}/(W^c_{PEO}\rho^c_{PEO} + W^a_{PEO}\rho^a_{PEO}) + M_n^{PS}/\rho_{PS}}$$

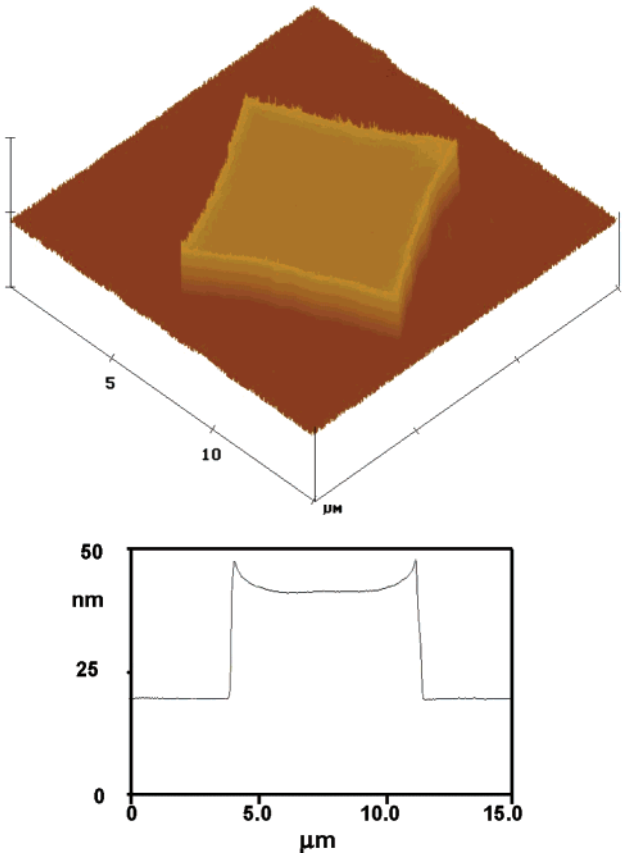

Figure 3. AFM height image of a square-shaped "sandwiched" single crystal of PEO-*b*-PS diblock copolymer (M_n^{PS} = 17K g/mol) crystallized at T_c = 30 °C in chlorobenzene/octane dilute solution. A height profile via cross-scanning the crystal is also included.

The d_{PEO} values of these three samples were calculated to be 11.4, 8.4, and 7.9 nm, respectively, for the three PEO-*b*-PS single crystals crystallized in the mixed solvent at 30 °C. Note that the calculation should only take the center thickness into account, in particular, for the PEO-*b*-PS with M_n^{PS} = 17K g/mol (see Figure 3). To verify the calculated data, the d_{PEO} was also measured via a seeding experiment. We used these PEO-*b*-PS single crystals as seeds for further crystal growth of a homo-PEO fraction in amyl acetate. The added homo-PEO molecules nucleate on the lateral {120} planes of the PEO-*b*-PS single crystal to grow homo-PEO single crystals. The initial thickness of these homo-PEO lamellar crystals epitaxially grown on the PEO block crystal can be measured using AFM. Since the initial thickness of the homo-PEO single crystals is identical to d_{PEO} of the copolymer crystal, the measurement is direct evidence of the d_{PEO} in the PEO-*b*-PS single crystal. In some of the AFM measurements, while depositing the crystals on to a hard silicon wafer surface, the homo-PEO single crystal slipped down to the silicon surface due to the gravity. Therefore, the thickness of the homo-PEO single crystal could be measured directly at/near the conjunction between the copolymer and homo-PEO single crystals, and the difference of the heights between the top surface of the diblock copolymer and the homo-PEO single crystal was then equal to $2d_{PS}$. To avoid this slippage, the single crystals were also deposited on a lightly cross-linked viscoelastic rubber substrate. In this case, the homo-PEO single crystal did not slip, and the difference of the heights between the top surface of the diblock copolymer and homo-PEO single crystal was then equal to d_{PS}. The d_{PS} and d_{PEO} values obtained in both types of measurements provide the identical results which agree with the calculated data using the equation. The d_{PS} values are thus 2.8 nm for M_n^{PS} = 4.6K g/mol, 5.2 nm for M_n^{PS} = 9.2K g/mol, and 7.2 nm for M_n^{PS} = 17K g/mol.

Since three values of M_n^{PEO} in the PEO-*b*-PS copolymers are 11K, 8.7K, and 11K g/mol, their average extended chain lengths with the 7_2 helix are 69.5, 55.0, and 69.5 nm, respectively.[33,34] Each PEO block can thus on average form 6, 7, and 9 stems in these three PEO-*b*-PS single crystals. Note that in the PEO crystal lattice each PEO stem occupies an area of 0.214 nm^2,[28] and hence, each PS block tethered on the basal surface of the PEO single crystal needs to cover an area of 2.57, 3.00, or 3.85 nm^2 for these three diblock copolymers, respectively (since in thermodynamic equilibrium, only 50% of the PS blocks are located at one side of the PEO block single crystal). The average tethering densities, σ, of the PS blocks on the basal surface of the PEO-*b*-PS single crystals for these three copolymers are thus correspondingly 0.39, 0.33, and 0.26 nm^{-2}. Since the values of d_{PS} are 2.8, 5.2, and 7.2 nm for these three diblock copolymers, each PS block with different M_n^{PS}s occupies a volume of 7.2, 15.6, and 27.7 nm^3, respectively. In the bulk PS samples with these three M_n^{PS}s, each PS molecule accordingly occupies a volume of 7.3, 14.5, or 26.8 nm^3 as calculated from the density data. Therefore, in the dry state, the PS block layer densities on the top and bottom do not deviate much from that in the bulk.

However, the fact that the PS block layer density is close to the PS bulk density does not imply that in the thin layers the PS blocks possess the same random coil conformation as in the PS bulk state. In the bulk state, PS having a M_n^{PS} = 4.6K, 9.2K, and 17K g/mol would have radii of gyration (R_g^{PS}) of 1.8, 2.6, and 3.6 nm (i.e., in the θ condition), respectively.[35] Examining the d_{PS}, it is found that, in the case of M_n^{PS} = 17K g/mol and M_n^{PS} = 9.2K g/mol, the d_{PS} is equal to $2R_g^{PS}$ (7.2 and 5.2 nm), indicating that the PS block conformation is close to the random coil in the bulk, while in the case of M_n^{PS} = 4.6K g/mol, the d_{PS} is only 78% of the $2R_g^{PS}$ (2.8 nm vs 3.6 nm), revealing that in this case the PS block conformation in the PS layers is a somewhat collapsed random coil.

Seeded Homo-PEO Crystal Growth. We used the PEO-*b*-PS single crystals as seeds to initiate homo-PEO crystal growth on the {120} growth fronts in amyl acetate dilute solution (note that amyl acetate is a very good solvent for PS). Figure 4 shows a BF TEM image of the self-seeded homo-PEO crystal growth when the seed was formed by the PEO-*b*-PS single crystal with M_n^{PS} = 4.6K g/mol. The four {120} growth fronts serve as nucleation sites to initiate the homo-PEO crystal growth. The oriented PE crystal rods on the homo-PEO crystal basal surface profile the four {120} sectors and the chain-folding directions are along the {120} planes.[23] On the other hand, the PE crystal rods are randomly oriented on the PEO-*b*-PS seed surface. Furthermore, the homo-PEO crystal is also a single crystal which possesses the same crystallographic orientation as the PEO-*b*-PS single crystal seed.

Figure 5 shows a BF TEM image of a seeded homo-PEO single crystal using the M_n^{PS} = 9.2K g/mol PEO-*b*-PS seed. It is surprising to observe that in this figure

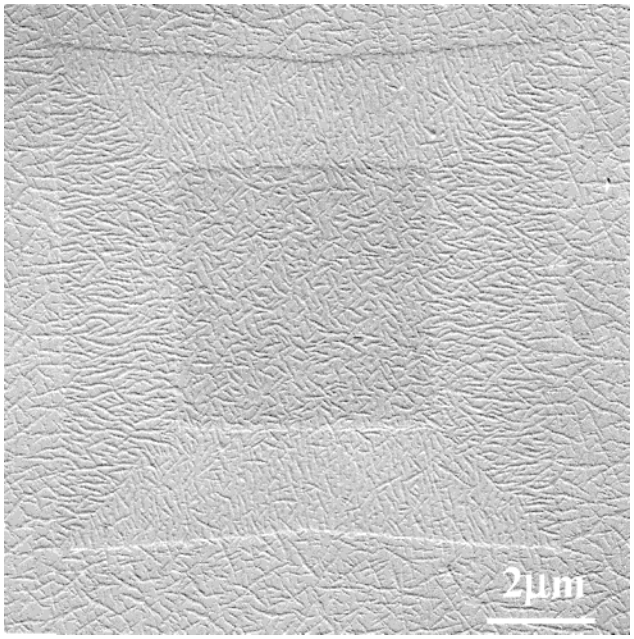

Figure 4. TEM BF image of the homo-PEO crystal growth on the PEO-*b*-PS diblock copolymer (M_n^{PS} = 4.6K g/mol) seed crystallized at T_c = 30 °C in amyl acetate dilute solution.

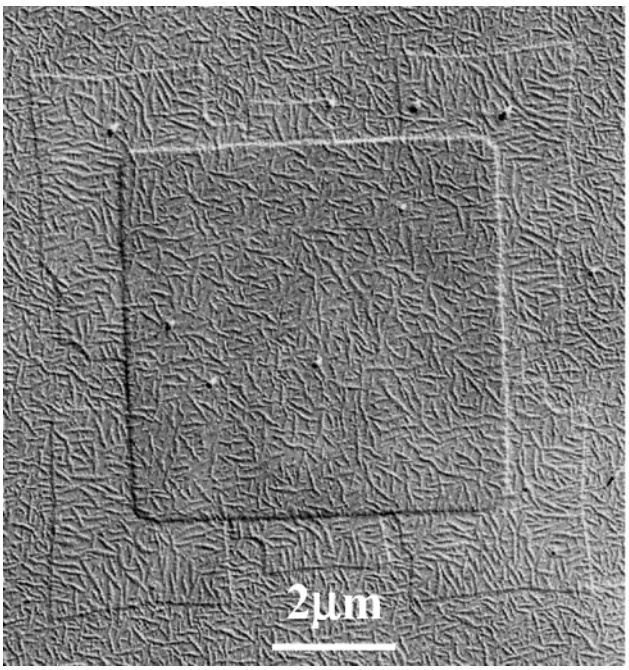

Figure 5. TEM BF image of the homo-PEO crystal growth on the PEO-*b*-PS diblock copolymer (M_n^{PS} = 9.2K g/mol) seed crystallized at T_c = 30 °C in amyl acetate dilute solution.

the homo-PEO can no longer grow uniformly along the {120} growth fronts of the PEO-*b*-PS single crystal seed. Rather, the four corners initiate the homo-PEO crystal growth first, and then, some sites along the edges initiate growth at later times as judged by their crystal sizes. Furthermore, the four corner PEO single crystals have the same size (isochronal nucleation). They seem to be coplanar with the parent crystal (the PEO-*b*-PS crystal), since these four crystals do not grow toward the parent crystal. The PE decoration indicates that these individual homo-PEO crystals are facetted single crystals with the {120} sectors. The chain-folding direction is also along the {120} planes. This reveals that

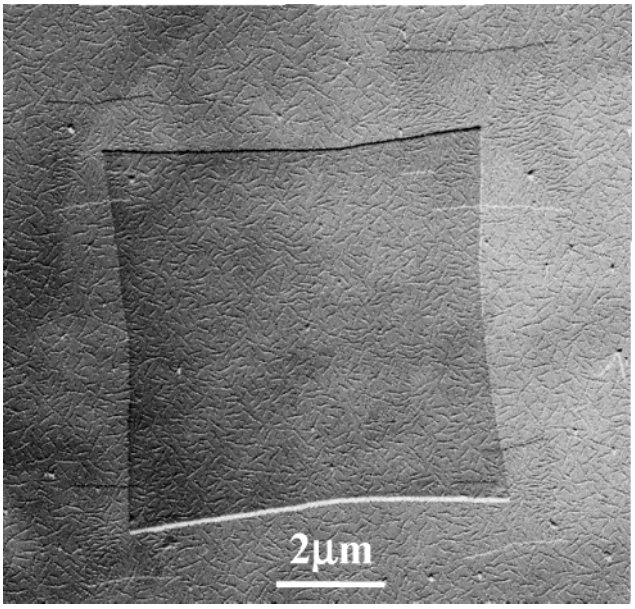

Figure 6. TEM BF image of the homo-PEO crystal growth on the PEO-*b*-PS diblock copolymer (M_n^{PS} = 17K g/mol) seed crystallized at T_c = 30 °C in amyl acetate dilute solution.

although each homo-PEO crystal grows independently at different times, the crystallographic orientation of the seeds is preserved.

When the M_n^{PS} of the PEO-*b*-PS single crystal increases to 17K g/mol, the homo-PEO crystal growth can only be initiated at the four corners as observed in a BF TEM image (Figure 6). The {120} edges can no longer provide any nucleation sites for the homo-PEO crystal growth. Moreover, among these homo-PEO single crystals at these four corners, one (at the right-up corner) is bigger than the others, indicating different initiation times of the nuclei. These homo-PEO single crystals also grow toward the parent crystal due possible to screw dislocations, and the growth back toward the parent crystal is much reduced compared to the outward growth. By comparing this figure with the observations in Figures 4 and 5, it is qualitatively concluded that increasing the M_n^{PS} causes the PS blocks in the PEO-*b*-PS single crystals to increasingly prevent the formation of nucleation and growth sites for the homo-PEO molecules on the {120} growth fronts.

How Do the PS Blocks Shield the Homo-PEO Crystal Growth? Based on our observations, when the tethered PS blocks are overcrowded and squeezed by the neighboring PS blocks to generate the lateral repulsion (i.e., a long enough M_n^{PS} and a high enough σ),[36,37] only those chains near or at the {120} growth fronts can partially release the repulsion force. This is because that the cumulated effect becomes high enough to push the PS blocks at the edges and corners beyond the PEO crystal growth front. It is similar to the "Skoulios effect".[36,37] The PS blocks are thus able to prevent the further crystallization of the homo-PEO by means of a "shielding" effect. However, when we put the seeds back into the PEO-*b*-PS/amyl acetate solution, the PEO-*b*-PS slowly grows again on the seeds. Why do the tethered PS block layers not stop the growth of the PEO-*b*-PS? We believe that this is critically dependent upon how the local chemical environment at the crystal growth front is constructed and what molecular interactions of the individual PEO-*b*-PS and homo-PEO are at the growth fronts.

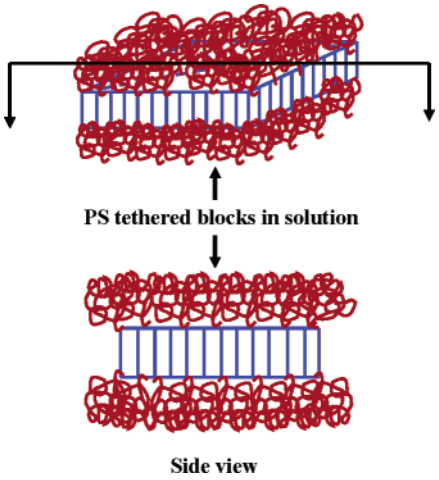

Figure 7. Schematic illustration of the PS block layer at the edge of the "sandwiched" crystal in solution. The PS blocks are pushed by their inner neighbors toward the [120] growth direction of the edges to form a PS block layer ahead of the PEO crystal growth fronts. The bottom carton represents the side view of the PEO-*b*-PS crystal.

Since the PEO-*b*-PS crystallization took place in amyl acetate, which is a very good solvent for PS, the PS blocks tethered on the basal surface of the PEO block single crystal must have conformations that are significantly more expanded compared with those in the chlorobenzene/octane mixed solvent (which is close to the θ condition).[38] Quantitatively, we use the simplified concept of reduced tethering density $\tilde{\sigma} = \sigma\pi R_g^2$ to illustrate how close the neighboring tethered PS chains are.[39] Here the R_g is the radius gyration of the PS of a particular M_n^{PS} in a particular solvent (here it is in amyl acetate).[39] Note that this $\tilde{\sigma}$ should be molecular weight and solvent independent. When the $M_n^{PS} = 4.6$K g/mol, the $\tilde{\sigma}$ of the tethered PS blocks in amyl acetate is 8.9. This value is higher than the value of $\tilde{\sigma}^* = 3.7-3.8$, which is the onset of PS blocks overcrowding by their neighbors.[32] However, further homo-PEO crystal growth is not shielded against on the edges and corners of the PEO-*b*-PS single crystal grown from the $M_n^{PS} = 4.6$K g/mol. This indicates that, in order to prevent the homo-PEO crystal growth on the PEO-*b*-PS seeds, the PS blocks require a much greater overcrowding and much stronger repulsion by neighboring PS blocks than those provided at the onset of overcrowding $\tilde{\sigma}^*$.

When the M_n^{PS} increases to $M_n^{PS} = 9.2$K g/mol for the PEO-*b*-PS single crystals, the $\tilde{\sigma}$ value is 17, and for the PEO-*b*-PS copolymer with $M_n^{PS} = 17$K g/mol, the $\tilde{\sigma} \sim 24$. These two $\tilde{\sigma}$ values may be within the highly stretched regime of the PS blocks. With increasing the M_n^{PS}, the repulsion force along the [120] growth directions becomes increasingly severe. The repulsion can only be partially released at the edges and corners of the single crystals by expanding themselves outward along the [120] directions when the PS blocks are tethered near and at the {120} edges and corners.

However, the PS blocks do not physically seal the PEO growth fronts in solution. Instead, the PS block layers advance ahead of the PEO growth fronts, as illustrated by the carton in Figure 7. In the case of PEO-*b*-PS crystallization, the PS blocks do not "welcome" the PEO blocks to be absorbed onto the PEO crystal growth front, but the PS blocks in the crystallizing PEO-*b*-PS molecules are compatible with the tethered PS blocks on the top and bottom of the PEO single crystal surface. The PS blocks are thus able to drag the PEO blocks to the growth front. The existing PS blocks in the PEO-*b*-PS molecules, hence, play an active role to assist the PEO blocks crystallizing onto the {120} growth fronts. This cannot take place with the homo-PEO on its own. Only at the sites where the $\tilde{\sigma}$ of the PS blocks is relatively small (such as the low $M_n^{PS} = 4.6$K g/mol) can the homo-PEO absorb to the PEO growth front and crystallize. This indicates that the local chemical environment, i.e., the "chemical shielding" at the growth front, does influence the PEO crystal growth and its kinetics, and this "shielding" effect becomes increasingly severe when the M_n^{PS} increases as shown in Figures 4−6.

The question that follows is, why is the nucleation of the homo-PEO less restricted at the corner than along the edge of the PEO-*b*-PS single crystal? Assuming the σ values of the tethered PS blocks along the edges and at the corners are identical, the overcrowded PS blocks at the edges may be pushed by their inner neighboring PS blocks toward the [120] growth direction that is perpendicular to the edge. However, the tethered PS blocks at the corners have two choices of where to expand since two edges merge at one corner. These results in a relatively small expansion of the PS block layers at the corners. Consequently, the homo-PEO molecules are relatively less prevented to grow at those corners. On the basis of this analysis, it is also evident that the solvent used in the crystallization should also affect the "chemical shielding" behavior since different solvents for the PS blocks generate different hydrodynamic volumes of the tethered PS blocks. This will change the value of σ and lead to a various degrees of repulsion. We will report our ongoing research along this direction in the near future.

Channel-Wire Arrays Having Chemical and Geometrical Recognitions. A direct result of this study is a new approach to fabricate channel-wire arrays having chemical and geometric recognitions via alternating crystal growth between the PEO-*b*-PS with $M_n^{PS} = 4.6$K g/mol and a homo-PEO using the lateral {120} surfaces of the preexisted crystals as seeds in dilute solution. Figures 8 and 9 show examples of this type of arrays in both BF TEM and AFM images, respectively. A SAED pattern of the [001] zone is also inserted in Figure 8, again indicating that the PEO chains in this alternating crystal possess a parallel orientation with respect to the basal surface normal. In these two figures, there is an alternating thickness change to achieve the geometric recognition. This is because the crystal thickness of the homo-PEO is thinner to form the channels (troughs), while the PS-*b*-PEO is thicker to form the wires (crests). The crests of the array are attributed to the PS blocks with a periodic thickness change of 2.8 nm. To precisely control the spacing size, knowledge of the growth rates of both homo-PEO and PEO-*b*-PS are critical as well as the crystallization times, concentrations, and solvent types. The lowest limit of spacing so far reached using this fabrication is 50 nm, as shown in Figure 10.

This channel-wire array also possesses alternating the chemical recognition. Since homo-PEO is hydrophilic and the PS is hydrophobic, we are able to create an environment with alternating hydrophilic channels and hydrophobic wires with controlled spacing and thicknesses on the array surface. This may provide a new way to investigate directional absorption, diffusion, and

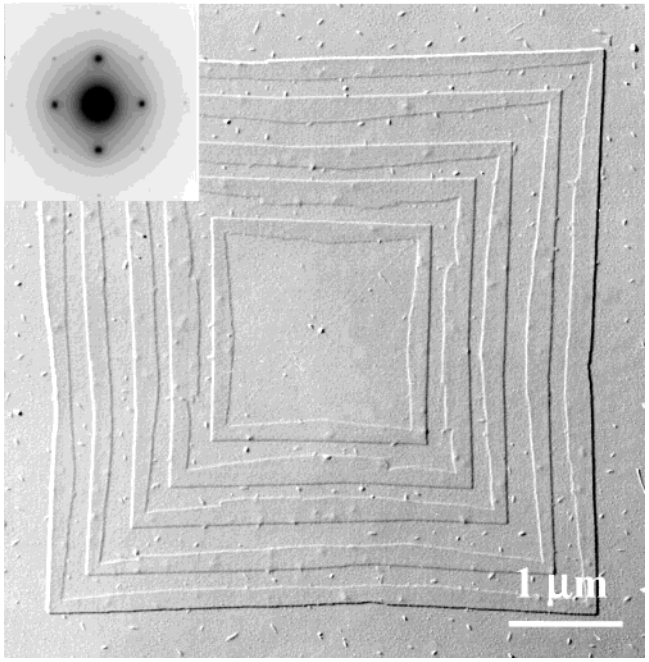

Figure 8. TEM BF image of a single crystal constructed by alternating PEO-*b*-PS and homo-PEO growths. The inset is a SAED pattern of this crystal in the correct orientation.

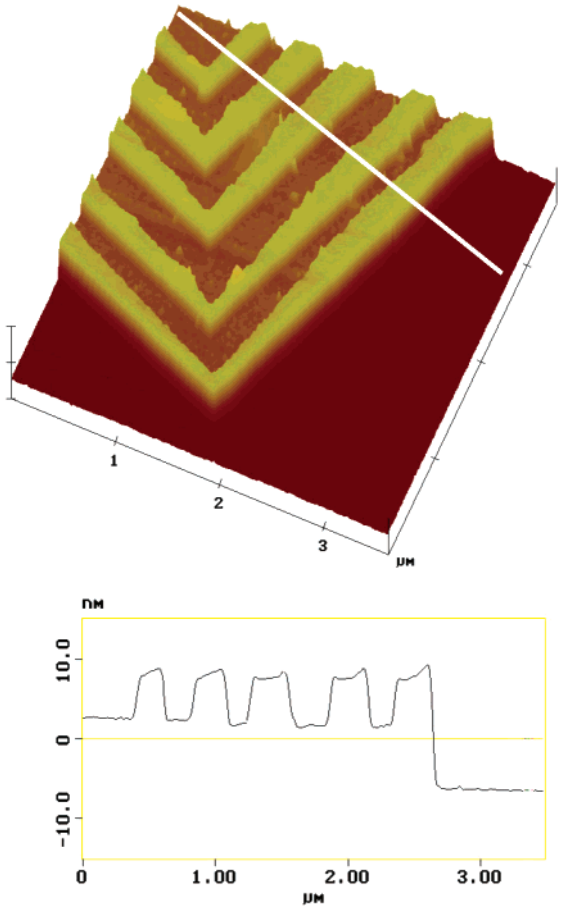

Figure 9. AFM height image of a single crystal constructed by alternating PEO-*b*-PS and homo-PEO growths.

immobilization of biomacromolecules on the array surface. It is also possible to increase the dielectric contrast of the arrays by selectively staining the polymers using RuO_4 or other reagents, as shown in Figure 11. Common

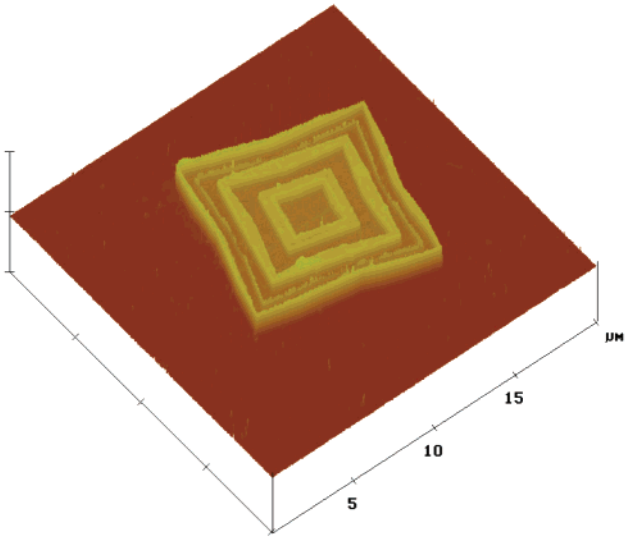

Figure 10. AFM height image of a single crystal constructed by alternating PEO-*b*-PS and homo-PEO growths with the smallest spacing of 50 nm.

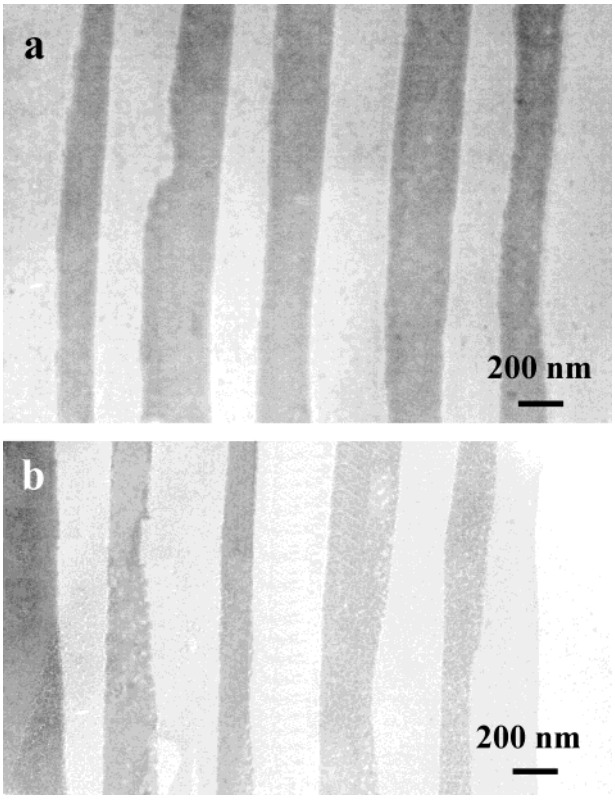

Figure 11. Two TEM BF images of the crystals with RuO_4 staining: (a) under a wet environment in which the PEO blocks were stained first and (b) under a dry environment in which the PS blocks were stained first.

understanding has been that both PS and PEO can be stained via RuO_4 oxidation, and staining PEO is generally viewed to be easier compared with PS.[40] It is interesting to find that the staining power of RuO_4 toward PEO and PS blocks is dependent upon the environment. When the environment is wet with a high humidity (created by a high vapor pressure), PEO blocks are stained first, but when the environment is dry with a low humidity (the sample and staining solution were protected in dry nitrogen), the PS blocks are stained first.

Conclusion

In summary, the PEO-*b*-PS diblock copolymers can grow "sandwiched" single crystals in dilute solution. When these single crystals are used as seeds to further grow homo-PEO, depending on the M_n^{PS} and $\tilde{\sigma}$ of the PEO-*b*-PS, the PS block may act as "chemically shielding" layers to hamper or even prevent the homo-PEO crystal growth. When $M_n^{PS} = 4.6$K g/mol, the PS blocks are overcrowded as evidenced by a $\tilde{\sigma} = 8.9$. However, all the edges and the corners of the PEO block single crystals can serve as nucleation sites for the further growth of the homo-PEO. This indicates that the generation of the "chemical shielding" requires a much stronger overcrowding compared with the onset of the overcrowding of $\tilde{\sigma}^* = 3.7-3.8$. With increasing the M_n^{PS} to 9.2K g/mol, the nucleation sites are limited to the corners and certain locations along the edges, and finally, only the corners can act as the nucleation sites for the further growth of the homo-PEO when the $M_n^{PS} = 17$K g/mol. This can be illustrated by an increase of the $\tilde{\sigma}$ value from 17 to 24. Therefore, the tethered PS blocks in amyl acetate (a very good solvent) possess very severe overcrowding and strong repulsion between the PS blocks and their neighbors. The tethered PS blocks at the edges are thus pushed by their inner neighbors toward the [120] growth direction of the growth fronts to form a PS layer ahead of the PEO crystal fronts. This advancement of the PS blocks in solution stops the growth of the homo-PEO, yet allows the further growth of the PEO-*b*-PS. When the single crystals of these PEO-*b*-PS copolymers are dried, the PS blocks solidify. The PS blocks at the edges and the corners possess less area for each PS block to cover, and therefore, the PS layers at the edges and the corners exhibit a slightly higher thickness compared to those in the center areas of the single crystals. As a direct result, the channel-wire arrays on the submicrometer length scale can be prepared via alternatively growing PEO-*b*-PS and homo-PEO crystals. This type of single crystal possesses an alternating thickness and an alternating hydrophobic−hydrophilic environment.

Acknowledgment. This work was supported by the NSF (Grant DMR-0203994).

References and Notes

(1) Frank, F. C.; Tosi, M. *Proc. R. Soc. London* **1961**, *A263*, 323.
(2) Hoffman, J. D.; Lauritzen, J. I., Jr. *J. Res. Natl. Bur. Stand.* **1961**, *65A*, 297.
(3) Hoffman, J. D.; Davis, G. T.; Lauritzen, J. I., Jr. In *Treasite on Solid State Chemistry*; Hannay, N. B., Ed.; Plenum: New York, 1976; Vol. 3, Chapter 7. For the recent development of the theory, see: Hoffman, J. D.; Miller, R. *Polymer* **1997**, *38*, 3151.
(4) For a comprehensive review, see: Armitstead, K.; Goldbeck-Wood, G. *Adv. Polym. Sci.* **1992**, *100*, 221.
(5) Cheng, S. Z. D.; Lotz, B. *Philos. Trans. A: Math. Phys. Eng. Sci. R. Soc. London* **2003**, *361*, 517.
(6) Pardey, R.; Wu, S. S.; Chen, J.-H.; Harris, F. W.; Cheng, S. Z. D.; Keller, A.; Aducci, J.; Facinelli, J. V.; Lenz, R. W. *Macromolecules* **1994**, *27*, 5794.
(7) Jing, A. J.; Taikum, O.; Li, C. Y.; Harris, F. W.; Cheng, S. Z. D. *Polymer* **2002**, *43*, 3431.
(8) Ungar, G.; Keller, A. *Polymer* **1987**, *28*, 1899.
(9) Organ, S. J.; Ungar, G.; Keller, A. *Macromolecules* **1989**, *22*, 1995.
(10) Cheng, S. Z. D.; Chen, J.-H. *J. Polym. Sci., Polym. Phys. Ed.* **1991**, *29*, 311.
(11) Ungar, G.; Mandal, P. K.; Higgs, P. G.; de Silva, D. S. M.; Boda, E.; Chen, C. M. *Phys. Rev. Lett.* **2000**, *85*, 4387.
(12) Alfonso, G. C.; Russell, T. P. *Macromolecules* **1986**, *19*, 1143.
(13) Di Lorenzo, M. L. *Prog. Polym. Sci.* **2003**, *28*, 663.
(14) Mareau, V. H.; Prud'homme, R. E. *Macromolecules* **2003**, *36*, 675.
(15) Zhu, L.; Cheng, S. Z. D.; Calhoun, B. H.; Ge, Q.; Quirk, R. P.; Thomas, E. L.; Hsiao, B. S.; Yeh, F.; Lotz, B. *J. Am. Chem. Soc.* **2000**, *122*, 5957.
(16) Huang, P.; Zhu, L.; Ge, Q.; Qiurk, R. P.; Cheng, S. Z. D.; Thomas, E. L.; Lotz, B.; Hsiao, B. S.; Yeh, F.; Liu, L. *Macromolecules* **2001**, *34*, 6649.
(17) Loo, Y.-L.; Register, R. A.; Ryan, A. J. *Phys. Rev. Lett.* **2000**, *84*, 4120.
(18) Zhu, L.; Huang, P.; Chen, W. Y.; Ge, Q.; Quirk, R. P.; Cheng, S. Z. D.; Thomas, E. L.; Lotz, B.; Hsiao, B. S.; Yeh, F.; Liu, L. *Macromolecules* **2002**, *35*, 3553.
(19) Lotz, B.; Kovacs, A. J. *Kolloid Z. Z. Polym.* **1966**, *209*, 97.
(20) Lotz, B.; Kovacs, A. J.; Bassett, G. A.; Keller, A. *Kolloid Z. Z. Polym.* **1966**, *209*, 115.
(21) Baltá Calleja, F. J.; Hay, I. L.; Keller, A. *J. Polym. Sci.* **1964**, *A2*, 2171.
(22) Baltá Calleja, F. J.; Hay, I. L.; Keller, A. *Colloid Z. Z. Polym. Sci.* **1966**, *209*, 128.
(23) Chen, J.; Cheng, S. Z. D.; Wu, S. S.; Lotz, B.; Wittmann, J.-C. *J. Polym. Sci., Polym. Phys. Ed.* **1995**, *33*, 1851−1855.
(24) Quirk, R. P.; Kim, J.; Kausch, C.; Chun, M. S. *Polym. Int.* **1996**, *39*, 3.
(25) Zhu, L.; Cheng, S. Z. D.; Calhoun, B. H.; Ge, Q.; Quirk, R. P.; Thomas, E. L.; Hsiao, B. S.; Yeh, F.; Lotz, B. *Polymer* **2001**, *42*, 5829.
(26) Wittmann, J.-C.; Lotz, B. *Makromol. Chim. Rapid Commun.* **1982**, *3*, 733.
(27) Wittmann, J.-C.; Lotz, B. *J. Polym. Sci., Polym. Phys. Ed.* **1985**, *23*, 205.
(28) Takahashi, Y.; Tadokoro, H. *Macromolecules* **1973**, *6*, 672.
(29) Based on our DSC measurements, the glass transition temperature of PS blocks was at 62 °C, and the melting temperature of the PEO block crystal was at 58 °C.
(30) Wunderlich, B. *Macromolecular Physics, Crystal Structure, Morphology, and Defects*; Academic: New York, 1973; Vol. 1.
(31) Our DSC experiments on collected "sandwiched" PEO-*b*-PS single crystals from amyl acetate solution showed that the heat of fusion under the melting endotherm of these crystals is 8.2 kJ/mol, which equivalent to 95% of the PEO crystallinity (the equilibrium heat of fusion is 8.66 kJ/mol). Note that this calculation needs to take the percentage of the PEO blocks in the diblock copolymer into account.
(32) Chen, W. Y.; Zheng, J. X.; Cheng, S. Z. D.; Li, C. Y.; Huang, P.; Zhu, L.; Xiong, H.; Ge, Q.; Guo, Y.; Quirk, R. P.; Lotz, B.; Deng, L.; Wu, C.; Thomas, E. L. *Phys. Rev. Lett.*, in press.
(33) Kovacs, A. J.; Lotz, B.; Keller, A. *J. Macromol. Sci., Phys.* **1969**, *3*, 385.
(34) Cheng, S. Z. D.; Wunderlich, B. *J. Polym. Sci., Polym. Phys. Ed.* **1986**, *24*, 1755.
(35) Arai, T.; Abe, F.; Yoshizaki, T.; Einaga, Y.; Yamakawa, H. *Macromolecules* **1995**, *28*, 5458.
(36) Raphaël, E.; de Gennes, P. G. *Makromol. Chem., Macromol. Symp.* **1992**, *62*, 1.
(37) Raphaël, E.; de Gennes, P. G. *Physica A* **1991**, *177*, 294.
(38) The second virial coefficient data of monodispersed PS (M_n^{PS} between 4.6K, 9.2K, and 17K g/mol) in amyl acetate solution were measured at 30 °C in one of our coauthor's (Prof. Chi Wu) laboratory at Hong Kong Chinese University. The values of R_g^{PS} for these PS samples were estimated from hydrodynamic radius in amyl acetate were 2.7, 4.1, and 5.4 nm, respectively. The results show that for PS chains amyl acetate is a very good solvent, which is about 6 times better than the mixed chlorobenzene/octane solvent (the mixed solvent is close to the θ condition).
(39) Kent, M. S. *Macromol. Rapid Commun.* **2000**, *21*, 243.
(40) Trent, J. S.; Scheinbeim, J. I.; Couchman, P. R. *Macromolecules* **1983**, *16*, 589.

MA0493325